Structural Engineering and Mechanics, Vol. 5, No. 1 (1997) 33-49
DOI: http://dx.doi.org/10.12989/sem.1997.5.1.033

Analysis of curved multicell box girder assemblages

A. Ghani Razaqpur†

Department of Civil and Environmental Engineering, Carleton University, 1125 Colonel By Dr., Ottawa, Ontario, R1S 586, Canada

Hangang Li‡

Proctor and Redfern Consulting Engineers, Toronto, Ontario, Canada

Abstract. A method of analysis is proposed for curved multicell box girder grillages. The method can be used to analyze box girder grillages comprising straight and/or curved segments. Each segment can be modelled by a number of beam elements. Each element has three nodes and the nodal degrees of freedom (DOF) consist of the six DOF for a conventional beam plus DOF to account for torsional warping, distortion,distortional warping, and shear lag. This element is an extension of a straight element that was developed earlier. For a more realistic analysis of the intersection regions of non-colinear box girder segments, the concept of a rigid connector is introduced, and the compatibility requirements between adjoining elements in those regions are discussed. The results of the analysis showed good agreement with the shell finite element results, but the proposed method of analysis needs a fraction of the time and effort compared to the shell finite element analysis.

Key words: analysis; beam; box girder; bridge; finite element; structures; thin-walled.

1. Introduction

Box girder grillages are sometimes used as bridges for modern roadway systems. The individual bridge segments may be straight or curved in plan and they may have single-cell or multicell cross-section. Fig. 1 illustrates a typical highway interchange where a single wide bridge bifurcates into two narrower bridges. It is the objective of this paper to address the analysis of box girder bridges belonging to this kind of structure. Such structures are difficult to analyze under the effect of general loading because conventional grillage methods of analysis are not capable of accounting for some important structural actions that are characteristic of thin-walled box girders. Conventional grillage analysis considers extension, flexure and torsion, but cross-sections of thin-walled box girders may warp out of the sectional plane and distort in the sectional plane. Also, shear lag effect may be significant in wide flange cross-sections and should be considered in design. For those reasons some bridge design codes (OHBD 1983) prohibit the use of conventional grillage analysis in the case of certain types of box girder bridges. As a consequence of the stated complexities, it has become customary to use finite strip or facet shell finite element idealizations to obtain box girder deformations and stresses. In spite of the rapid progress in

† Professor
‡ Senior Bridge Designer

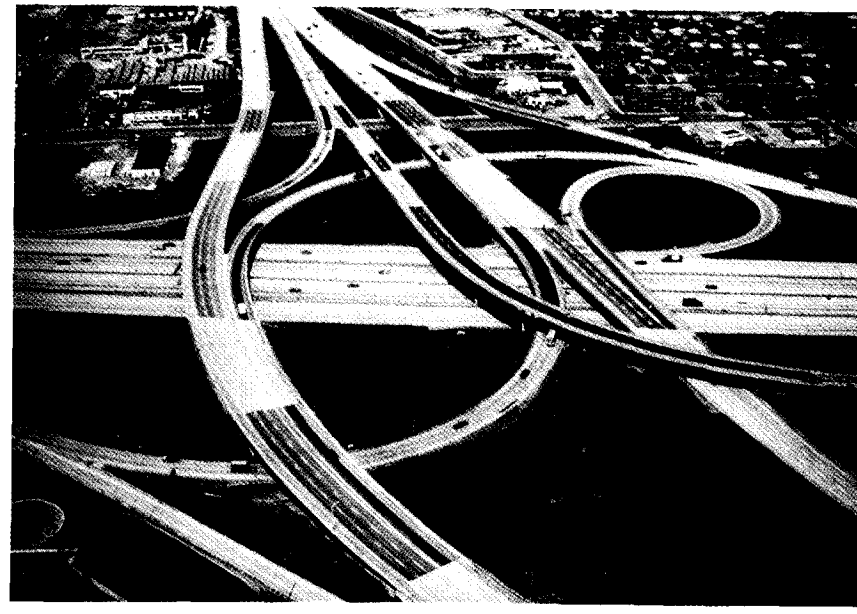

Fig. 1 Typical box girder assemblage.

high-speed computation, however, due to the large number of degrees of freedom needed for proper modelling, detailed three dimensional finite element analysis of box girders is still too expensive and time consuming. Thus, it is important to develop a suitable box beam element that includes all of the above structural actions and which could be used to model box girder grillages.

In the past several investigations have been undertaken to develop such elements. Bazant and El Nimeiri (1974) developed a skew thin-walled box beam finite element for curved single-cell box girders in which distortion and torsional warping were considered. A similar approach was adopted by Mikkola and Paavola (1980) while Zhang and Lyons (1984) developed a thin-walled multicell box beam finite element. They considered only one distortioned mode even for multicell boxes and they modelled shear lag using the simplified concept of effective width. Sedlacek (1968), and Roik and Sedlacek (1970) used rigorous analytical procedures to extend Vlasov's thin-walled beam to multicell boxes by considering the effects of cross-sectional distortion, distortional warping and shear lag. Based on this extended theory, Razaqpur and Li (1991 and 1994) developed two multi-cell box girder finite element models, one for straight box beams based on exact shape functions, and the other for curved box beams based on conventional polynomial shape functions. In a previous study it was shown how straight box girder grillages can be modelled (Razaqpur and Li 1990) using the proposed method. It is the purpose of the present paper to extend the application of these elements to the analysis of multicell horizontally curved box girder grillages, comprising straight and/or curved segments, and to show how one can model the intersection regions of box girder segments in order to avoid some of the complexities inherent in those regions.

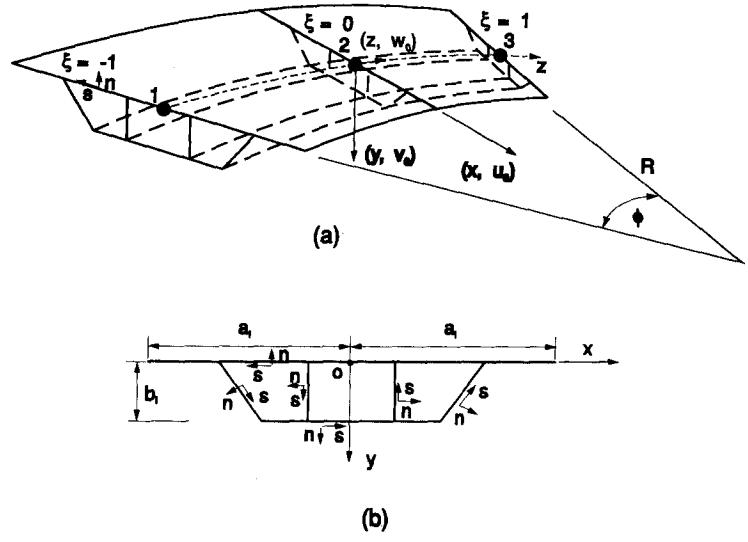

Fig. 2 Geometry of curved multicell beam box element.
(a) Curved multicell beam box finite element
(b) Multicell box cross-section and local coordinate system

2. Mechanics of curved multicell box girders

Fig. 2 illustrates a typical multicell box girder, and its flange and web plates. In addition to the element coordinate system x, y and z shown in Fig. 2(a), for each plate a local coordinate system z, s and n is introduced, Fig. 2(b), in such a way that the z-axis and the element axis would be parallel and the s and n-axes would be tangent and normal to the middle plane of the wall plate, respectively. Note that z is a curved circumferential axis and that the position of origin 0 of the x, y and z axes is arbitrarily selected but is assumed here to lie on the middle plane of the top slab. The wall contour coordinate, s, is measured from point 0 and is assumed positive counterclockwise.

For simplicity, we shall start with the kinematics of deformation of a single cell box girder with curvature χ. The displacement components $w(s, z)$, $v_s(s, z)$ and $v_n(s, z)$ in the z, s and n directions, respectively, of a point $S(s, z)$, Fig. 2(b) can be written as (Razaqpur and Li 1994)

$$w(s, z)=w_0+y\theta_x-x(\theta_y+w_0\chi)-\omega(\theta_z'-\theta_x\chi)-\omega_d\beta'-\omega_{s1}\eta_1'-\omega_{s2}\eta_2'-\omega_{s3}\eta_3' \tag{1a}$$

$$v_s(s, z)=\Psi_1 u_0+\Psi_2 v_0+p(s)\theta_z+\Psi_d\beta \tag{1b}$$

$$v_n(s, z)=\Omega_1 u_0+\Omega_2 v_0+\Omega(6)\theta_z+\Omega_d\beta \tag{1c}$$

where u_0, v_0 and w_0 are the x, y and z displacements of reference point 0, θ_x and θ_y are the combined flexural and shear rotations of the cross-section about the x and y, respectively, θ_z is the angle of twist, $p(s)$ is the distance from 0 to the tangent of the middle plane at S, ω is the torsional warping function (sectorial coordinate) with respect to pole 0, and prime over the symbols denotes derivative with respect to z. The third and fourth terms of Eq. (1a), respectively, account for the fact that in a curved box girder circumferential extension of the box axis causes

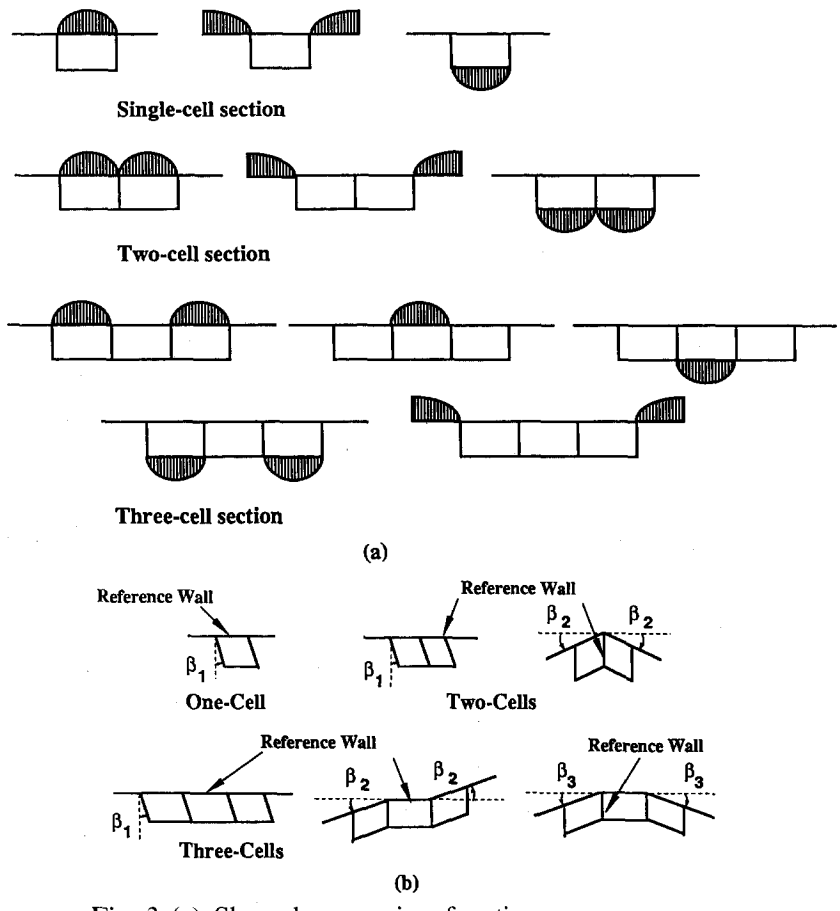

Fig. 3 (a) Shear lag warping functions.
(b) Distortional modes of multicell box girder

rotation about the y-axis while rotation about the x-axis produces twisting (Li 1987). The latter is the well-known coupling of bending and twisting actions in a horizontally curved bar.

In Eq. 1(a) to 1(c) besides the generalized displacements u_0, v_0, w_0, θ_x, θ_y and θ_z, we observe the generalized displacements β and η_i ($i=1, 3$), or their derivatives. The quantity β is the angle of distortion of the box section and ω_d is its associated warping function; η_i is a function which describes the variation of shear lag warping as a function of z, while the functions ω_{si} ($i=1, 3$) describes its variation with coordinate s. It should be emphasized that shear lag is considered to be important only in the top and bottom slabs and their overhangs. Following Reissner's hypothesis (1938), functions ω_{si} are assumed to be parabolic as illustrated in Fig. 3(a).

The functions Ψ_1, Ψ_2, Ω_1 and Ω_2 are actually the direction cosines of s and n, respectively, with respect to x and y, while Ψ_d and Ω_d are functions which describe the s and n components of the displacement of point S due to distortion β. In Eq. 1(a) to 1(c) it is implicit that $R/b \geq 10$, where R is the radius of curvature of the box girder and b is the width of the top slab. As shown by Li (1987), when the preceding condition is satisfied, it is sufficiently accurate to assume that the neutral axis of a curved box coincides with its centroidal axis and the centroidal radius represents the curvature of the entire cross-section.

Eqs. 1(a) to 1(c) may be cast in matrix form as:

$$w(s, z)=\{\Phi_1\}\{D\}+\{\Phi_2\}\{D\}' \tag{2a}$$

$$v_s(s, z)=\{\Psi\}\{D\} \tag{2b}$$

$$v_s(s, z)=\{\Omega\}\{D\} \tag{2c}$$

where

$$\{D\}=\{u_0, v_0, w_0, \theta_x, \theta_y, \theta_z, \beta, \eta_1, \eta_2, \eta_3\}^T \tag{3a}$$

$$\{\Phi_1(s)\}=[0, 0, (1-x\chi), (y+\omega\chi), -x, 0, 0, 0, 0, 0] \tag{3b}$$

$$\{\Phi_2(s)\}=[0, 0, 0, 0, 0, -\omega, -\omega_d, -\omega_{s1}, -\omega_{s2}, -\omega_{s3}] \tag{3c}$$

$$\{\Psi\}=[\Psi_1, \Psi_2, 0, 0, 0, \rho(s), \Psi_d, 0, 0, 0] \tag{3d}$$

$$\{\Omega\}=[\Omega_1, \Omega_2, 0, 0, 0, \Omega_6, \Omega_d, 0, 0, 0] \tag{3e}$$

Note that $\{\Phi_1\}$, $\{\Phi_2\}$, $\{\Psi\}$ and $\{\Omega\}$ are functions of s only while $\{D\}$ is a function of z alone; hence, the box displacements are conveniently expressed using the separation of variables.

In a multicell box, extension, bending and twisting can be expressed in terms of the same generalized displacements as used for a single cell box, but the shear lag and distortion would require consideration of additional deformation modes. The procedure for shear lag is the same as before, i.e., parabolic warping functions ω_{si} will be used for each slab plate (top and bottom of each cell and for each slab overhang). Hence the total number of displacement functions η_i for shear lag warping is $k=2j+1$, where j=total number of cells in a single spine multicell box, Fig. 3(a). For multicell cross-sections symmetric with respect to the y-axis, $k=(2j-1)$ (Razaqpur and Li 1994).

The distortion of a multicell box is somewhat complicated; however, Maisel (1982) showed that a conservative estimate of distortional warping stresses could be obtained if shear deformations in the planes of the walls were neglected in the distortional analysis. Based on that assumption, he indicated that the distortional warping of a multicell box can be approximated by decomposing the actual distortion into j linearly independent distortional modes, each of which can be characterized by a warping function ω_{di} $(i=1, j)$ and the associated distortional angle β_i. For single spine box girders, j is equal to the number of cells in the box, Fig. 3(b). Note that β_i is measured from an arbitrary reference wall.

In the light of the preceding discussion, and by reference to Eq. 2(a) to (c), the displacement components of a point on the middle plane of a wall of a multicell box girder can be written in the form of Eq. 2(a) to 2(c), as in the case of a single cell box, but the pertinent vectors will be

$$\{D\}=\{u_0, v_0, w_0, \theta_x, \theta_y, \theta_z, \beta_1, \beta_2, \cdots, \beta_j, \eta_1, \eta_2, \cdots, \eta_k\}^T \tag{4a}$$

$$\{\Phi_1(s)\}=[0, 0, (1-x\chi), (y+\omega\chi), -x, 0, 0, \cdots, 0, 0, \cdots, 0] \tag{4b}$$

$$\{\Phi_2\}=[0, 0, 0, 0, 0, -\omega, -\omega_{d1}, -\omega_{d2}, \cdots, -\omega_{dj}, -\omega_{s1}, -\omega_{s2}, \cdots, -\omega_{sk}] \tag{4c}$$

$$\{\Psi\}=[\Psi_1, \Psi_2, 0, 0, 0, \rho(s), \Psi_{d1}, \Psi_{d2}, \cdots;, \Psi_{d2}, \cdots, \Psi_{dj}, 0, 0, \cdots, 0] \tag{4d}$$

$$\{\Omega\}=[\Omega_1, \Omega_2, 0, 0, 0, \Omega_6, \Omega_{d1}, \Omega_{d2}, \cdots, \Omega_{dj}, 0, 0, \cdots, 0] \tag{4e}$$

By comparing the vectors in Eq. 4(a) to 4(e) with the corresponding vectors in Eq. 3(a) to 3(e)

where

$$[B_1]=\begin{Bmatrix} 0 \\ \{\dot{\Psi}\}-n\{\ddot{\Omega}\} \\ \{\dot{\Phi}_1\} \end{Bmatrix} \tag{9a}$$

$$[B_2]=\begin{Bmatrix} \{\Phi_1\} \\ 0 \\ \{\dot{\Phi}_2\}+\{\Psi\}-2n\{\dot{\Omega}\} \end{Bmatrix} \tag{9b}$$

$$[B_3]=\begin{Bmatrix} \{\Phi_2\}-n\{\Omega\} \\ 0 \\ 0 \end{Bmatrix} \tag{9c}$$

The stress-strain relationship is given by

$$\{\sigma\}=[E]\{\varepsilon\}=[E](\{B_1\}\{D\}+[B_2]\{D\}'+[B_3]\{D\}'') \tag{10}$$

where $\{\sigma\}$ is the vector of normal and shear stresses and $[E]$ is the elasticity matrix, i.e.

$$\{\sigma\}=[\sigma_z,\ \sigma_s,\ \tau_{sz}]^T \tag{11}$$

$$[E]=\frac{1}{1-\nu_z\nu_s}\begin{bmatrix} E_z & \nu_z E_z & 0 \\ \nu_s E_s & E_s & 0 \\ 0 & 0 & (1-\nu_z\nu_s)G \end{bmatrix} \tag{12}$$

where E_z and E_s are Young's moduli in the longitudinal and transverse directions respectively; ν_z and ν_s are the Poisson's ratios in the z and s directions, and $\nu_z E_z=\nu_s E_s$. Note that in conventional beam theory σ_s is generally assumed to be negligible.

3. Finite element formulation

The ordinary differential equation governing axial extention of an Euler-Bernoulli beam is second order while those governing bending and Wagner's torsion are fourth order. It can be shown (Razaqpur and Li 1991) that the governing equations of distortion and shear lag are also fourth order. In the present analysis, we will use Timoshenko's beam theory; hence, the generalized displacements required to model the foregoing actions would be those given in Eq. 4(a), where the rotations θ_x and θ_y are considered to be independent variables. In the following we will develop a three node multicell box beam finite element employing the generalized displacements of Eq. 4(a).

Consider a one dimensional beam element with three nodes as in Fig. 2. Its stiffness matrix and nodal load vector are first developed based on the degrees of freedom for three nodes. Subsequently, a static condensation technique can be used to eliminate the degrees of freedom corresponding to the middle node 2. The complete vector of element nodal degrees of freedom, $\{D\}^e$ is given by

$$\{D\}^e=[u_1,\ u_2,\ u_3,\ v_1,\ v_2,\ v_3,\ w_1,\ w_2,\ w_3,\ \theta_{x1},\ \theta_{x2},\ \theta_{x3},$$

for a single cell box girder, we observe that the extension, bending and twisting of a curved multicell box girder can be represented by the same six generalized displacements as in a single cell box, but the distortion and shear lag require consideration of a greater number of deformation modes as represented by $\beta_i (i=1, j)$ and η_i $(i=1, k)$.

Considering the out of plane bending of the walls, the displacement components of an arbitrary point of the cross section with coordinates (s, z, n) can be expressed as:

$$w(s, z, n)=w(s, z)-n\frac{\partial v_n(s, z)}{\partial z} \tag{5a}$$

$$v_s(s, z, n)=v_s(s, z)-n\frac{\partial v_n(s, z)}{\partial s} \tag{5b}$$

$$v_n(s, z, n)=v_n(s, z) \tag{5c}$$

where n is the perpendicular distance of the point under consideration from the middle plane of the wall. Substituting Eqs. (2a) to (2c) into Eqs. (5a) to (5c), the following matrix equations can be written

$$\begin{Bmatrix} w(s, z, n) \\ v_s(s, z, n) \\ v_n(s, z, n) \end{Bmatrix}=\{A_1\}\{D\}+\{A_2\}\{D\}' \tag{6a}$$

$$\{A_1\}=\begin{Bmatrix} \{\Phi_1\} \\ \{\Psi\}-n\{\dot{\Omega}\} \\ \{\Omega\} \end{Bmatrix} \tag{6b}$$

$$\{A_2\}=\begin{Bmatrix} \{\Phi_2\}-n\{\Omega\} \\ 0 \\ 0 \end{Bmatrix} \tag{6c}$$

where superscript dot denotes derivative with respect to coordinate s. Based on the small deformation theory of linear elasticity, the normal and shear strains may be determined using

$$\varepsilon_z=\frac{\partial w(s, z, n)}{\partial z}=\frac{\partial w(s, z)}{\partial z}-n\frac{\partial^2 v_n(s, z)}{\partial z^2} \tag{7a}$$

$$\varepsilon_s=\frac{\partial v_s(s, z)}{\partial s}-n\frac{\partial^2 v_n(s, z)}{\partial s^2} \tag{7b}$$

$$\gamma_{sz}=\frac{\partial w(s, z)}{\partial s}+\frac{\partial v_s(s, z)}{\partial z}-2n\frac{\partial^2 v_n(s, z)}{\partial z\,\partial s} \tag{7c}$$

Substituting Eqs. (6a) to (6c) into Eqs. (7a) to (7c), the strain vector can be obtained

$$\begin{Bmatrix} \varepsilon_z \\ \varepsilon_s \\ \gamma_{sz} \end{Bmatrix}=[B_1]\ \{D\}+[B_2]\{D\}'+[B_3]\{D\}'' \tag{8}$$

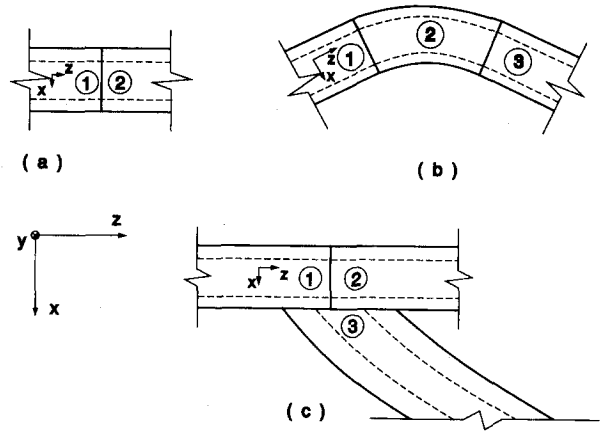

Fig. 4 Typical intersection of box girder bridge assembladges in plan.
(a) Two colinear straight segments
(b) Straight segments joining a curved segment
(c) Segments intersecting at an angle

$$\theta_{y1},\ \theta_{y2},\ \theta_{y3},\ \theta_{z1},\ \theta'_{z1},\ \theta_{z2},\ \theta'_{z2},\ \theta_{z3},\ \theta'_{z3},$$
$$\beta_{11},\ \beta'_{11},\ \beta_{12},\ \beta'_{12},\ \beta_{13},\ \beta'_{13},\ \cdots,\ \beta_{j1},\ \beta'_{j1},\ \beta_{j2},\ \beta'_{j2},\ \beta_{j3},\ \beta'_{j3},$$
$$\eta_{11},\ \eta'_{11},\ \eta_{12},\ \eta'_{12},\ \eta_{13},\ \eta'_{13},\ \cdots,\ \eta_{k1},\ \eta'_{k1},\ \eta_{k2},\ \eta'_{k2},\ \eta_{k3},\ \eta'_{k3}]^T \tag{13}$$

In the above the first subscript represents the generalized displacement component or its derivative while the second subscript refers to the node number. It must be emphasized that vector $\{D\}^e$ represents nodal DOF which consist of the generalized displacements in vector $\{D\}$ or their derivatives. Since Timoshenko's beam theory is used for bending analysis, for extensional, flexural and torsional effects, C_0 continuity is required and thus parabolic shape functions N_i will be used.

$$N_i=\frac{1}{2}(\xi^2+\xi_0) \qquad (i=1,\ 3) \tag{14}$$

$$N_i=(1-\xi^2) \qquad (i=2) \tag{15}$$

where $\xi_0=\xi\xi_i$, is the node number, and ξ is a natural coordinate with value of -1, 0, $+1$ at nodes 1,2 and 3 respectively.

For distortional and shear lag effects, C_1 continuity is required, thus the following shape functions are used. For nodes 1 and 3 ($i=1,\ 3$)

$$N_{i1}=\frac{\xi^2}{4}(4+5\xi_0-2\xi^2-3\xi_0^3) \quad (i=1,\ 3) \tag{16}$$

$$N_{i2}=\frac{J_i}{4}\xi^2(1+\xi_0)(1-\xi^2) \tag{17}$$

For node 2

$$N_{21}=(1-\xi^2)^2 \qquad (i=2) \tag{18}$$

$$N_{22}=J\xi(1-\xi^2)^2 \tag{19}$$

where

$$J=\frac{\partial x}{\partial \xi}. \tag{20}$$

and N_{ij} are shape functions.

The element displacements, $\{D\}$, can be related to its nodal degrees of freedom, $\{D\}^e$, by

$$\{D\}=[N]\{D\}^e \tag{21}$$

where $[N]$ is the shape function matrix. The matrix $[N]$ for the proposed element will have the form

$$[N]=\begin{bmatrix} [N]_1 & [N]_2 & \cdots & [N]_7 & [N]_{d1} & & \cdots & [N]_{dj} & [N]_{s1} & \cdots & [N]_{sk} \end{bmatrix} \tag{22}$$

in which

$$[N]_i=[N_1\ N_2\ N_3] \quad (i=1 \text{ to } 7);$$
$$[N]_i=[N_{11}\ N_{12}\ N_{21}\ N_{22}\ N_{31}\ N_{32}] \quad (i=d1 \text{ to } sk).$$

Substituting Eq. (21) into Eq. (8) gives

$$\{\varepsilon\}=[B]\{D\}^e \tag{23}$$

where $[B]$ is the strain-displacement matrix

$$[B]=\begin{Bmatrix} \{\Phi_1\}[N]'+(\{\Phi_2\}-n\{\Omega\})[N]'' \\ -n\{\ddot{\Omega}\}[N] \\ \{\dot{\Phi}_1\}[N]+(\{\dot{\Phi}_2\}+\{\Psi\}-2n\{\dot{\Omega}\})[N]' \end{Bmatrix} \tag{24}$$

The element stiffness matrix, $[S]^e$, and the equivalent nodal load vector, $\{F\}^e$, can be found from the virtual work principle

$$[S]^e=\int_V [B]^T[E][B]\,dv=\int_{-1}^{+1}\int_0^{+1}\int_{\xi_1}^{\xi_2}[B]^T[E][B]|J|d\xi d\eta d\zeta \tag{25}$$

$$\{F\}^e=\int_V([N]^T\{A_1\}^T+[N]'^T\{A_2\}^T)\{F\}\,dv$$
$$\int_S([N]^T\{A_1\}^T+[N]'^T\{A_2\}^T)\{T\}\,dS$$
$$\sum([N]^T\{A_1\}^T+[N]'^T\{A_2\}^T)\{P\} \tag{26}$$

where $\{F\}=[F_z, F_s, F_n]^T$ and $\{T\}=[T_z\ T_s\ T_n]^T$ are the body forces load vector and surface loads vector, respectively; $\{P\}=[P_z\ P_s\ P_n]^T$ is the applied concentrated loads vector, η and ζ are natural coordinates and $|J|$ is the Jacobian. Eqs. (25) and (26) can be integrated using Gaussian integration.

Once the element stiffness matrix and equivalent nodal load vectors have been found, the final solution, such as the distribution of displacements and stresses within the structures can be obtained by procedures commonly used in the finite element method.

4. Box girder grillage

Through appropriate coordinate transformation, the finite element model developed in this paper can be used to analyze multicell and multi-branch box girder structures. Consider the box girder grillages in Fig. 4, which shows how two or three different segments join in a box girder assemblage. Fig. 4(a) shows two straight box girder segments joined together while in Fig. 4(b) straight segments 1 and 3 join the curved segment 2, and in Fig. 4(c) segment 3 intersects segments 1 and 2 at an angle. Combinations of these three types of intersecting box assemblages may also occur in practice. The actual state of stresses in these intersection zones may be rather complex and may need detailed finite element analysis using shell elements. The global effects can be, however, considered using the method proposed herein.

First, modelling any complex three dimensional structure by a grillage of one dimensional beam elements creates some approximations. The degree of approximation in part depends on the relative dimensions of the beam elements. In building frames, joint dimensions are generally ignored in analysis because they are thought to be much smaller than the pertinent beam and column lengths. In the case of box girder grillages, using the centerline dimensions of each box girder segment to construct the grillage may introduce spurious element dimensions because in reality box girder segments may not be collinear, in which case they join each other at the outside surfaces of their webs, and the extra length from the outer web to the centerline may be quite large. Hence to improve the modelling, it is proposed to use the actual length of each box girder segment in the analysis.

If the ends of the segments do not actually meet, for the purposes of modelling they are assumed to be connected by means of a rigid arm, subject to the inter-element compatibility requirements to be discussed below. The compatibility conditions of the joints connecting the individual box girder elements are dependent on the type of connection. In Fig. 4(a), elements 1 and 2 are both straight elements and have the same cross section and their ends actually meet; hence there is complete structural and geometric continuity at the elements intersection, thus compatibility would be enforced for all the common nodal degrees of freedom. Fig. 3(b) illustrates the case of a curved element meeting a straight element at an angle. In this case, we enforce continuity of u, v, w, θ_z, θ_y and θ_x. This degree of continuity is identical to that required in conventional beam grillages. The other degrees of freedom, such as torsional warping θ_z', distortion β_i, distortional warping β_i', shear lag η_i and shear lag warping η_i', are treated as local degrees of freedom, reflecting the local deformations of the individual cross sections. Those degrees of freedom for which continuity must be enforced are therefore transformed to a common global coordinate system. Fig. 4(c) is the combination of Fig. 4(a) and 4(b), which shows that between elements 1 and 2 full continuity is maintained while between element 3 and the preceding two elements only partial continuity is enforced as in Fig. 4(b).

After the elimination of the middle node degrees of freedom by static condensation for the curved box beam element, the nodal degrees of freedom become

$$\{D_c\}^e=[u_1,\ v_1,\ w_1,\ \theta_{x1},\ \theta_{y1},\ \theta_{z1},\ \theta'_{z1},\ \beta_{11},\ \beta'_{11},\ \cdots,\ \beta_{j1},\ \beta'_{j1},\ \eta_{11},\ \eta'_{11},\ \cdots,\ \eta_{k1},\ \eta'_{k1},$$
$$u_3,\ v_3,\ w_3,\ \theta_{x3},\ \theta_{y3},\ \theta_{z3},\ \theta'_{z3},\ \beta_{13},\ \beta'_{13},\ \cdots,\ \beta_{j3},\ \beta'_{j3},\ \eta_{13},\ \eta'_{13},\ \cdots,\ \eta_{k3},\ \eta'_{k3}]^T \quad (27)$$

In the straight box girder finite element developed earlier by Razaqpur and Li (1991) element nodes are assumed to be located along the centroidal axis of the box girder while for torsion they are considered to be located on an axis parallel to the centroidal axis but passing through the shear center. Furthermore, the straight element did not account for shear deformations. In the present curved element, the nodes are located on an axis parallel to the centroidal axis but going through an arbitrary point 0 in the top slab. In view of this difference in the position of the nodes of the two types of elements, the continuity conditions at the junction of a straight and a curved element satisfy the following conditions:

$$\bar{u}=u_0-y_s\theta_z \quad (28a)$$

$$\bar{v}=v_0 \quad (28b)$$

$$\bar{w}=w_0-y_c v\theta_x+\omega\,\theta_z+\omega_{d1}\beta_1+\cdots+\omega_{dj}\beta_j+\omega_{s1}\eta_1+\cdots+\omega_{sk}\eta_k \quad (28c)$$

$$\bar{\theta}_x=\theta_x \quad (28d)$$

$$\bar{\theta}_y=\theta_y+y_c\theta_z' \quad (28e)$$

$$\bar{\theta}_z=\theta_z \quad (28f)$$

$$\bar{\beta}_1=\beta_1 \quad (28g)$$

$$\bar{\beta}_j=\beta_j \quad (28h)$$

$$\bar{\eta}_1=\eta_1 \quad (28i)$$

$$\bar{\eta}_k=\eta_k \quad (28j)$$

In which y_c and y_s are the y coordinates of the centroid and the shear center of the box cross-section, respectively.

In Eqs. 28(a) to 28(j) the quantities on the left-hand side of these equations belong to the straight box girder while those on the right-hand side belong to the curved box girder. Thus, the transformation between the nodal degrees of freedom can be expressed as

$$\{D\}^e=[T_{sc}]\,\{D_c\}^e \quad (29)$$

with

$$[T_{sc}]=\begin{bmatrix}[t_{sc}] & \\ & [t_{sc}]\end{bmatrix} \quad (30)$$

where the submatrix $[t_{sc}]$ as follows

$$[t_{sc}]=\begin{bmatrix}
1&0&0&0&0&y_s&0&0&0&\cdots&0&0&0&0&\cdots&0&0\\
0&1&0&0&0&0&0&0&0&\cdots&0&0&0&0&\cdots&0&0\\
0&0&1&-y_c&0&\omega&0&\omega_{d1}&0&\cdots&\omega_{dj}&0&\omega_{s1}&0&\cdots&\omega_{sk}&0\\
0&0&0&1&0&0&0&0&0&\cdots&0&0&0&0&\cdots&0&0\\
0&0&0&0&1&0&y_c&0&0&\cdots&0&0&0&0&\cdots&0&0\\
0&0&0&0&0&1&0&0&0&\cdots&0&0&0&0&\cdots&0&0\\
0&0&0&0&0&0&1&0&0&\cdots&0&0&0&0&\cdots&0&0\\
0&0&0&0&0&0&0&1&0&\cdots&0&0&0&0&\cdots&0&0\\
0&0&0&0&0&0&0&0&1&\cdots&0&0&0&0&\cdots&0&0\\
\cdots&\cdots&\cdots&\cdots&\cdots&\cdots&\cdots&\cdots&\cdots&1&\cdots&\cdots&\cdots&\cdots&\cdots&\cdots&\cdots\\
\cdots&\cdots&\cdots&\cdots&\cdots&\cdots&\cdots&\cdots&\cdots&1&\cdots&\cdots&\cdots&\cdots&\cdots&\cdots&\cdots\\
\cdots&\cdots&\cdots&\cdots&\cdots&\cdots&\cdots&\cdots&\cdots&1&\cdots&\cdots&\cdots&\cdots&\cdots&\cdots&\cdots\\
0&0&0&0&0&0&0&0&0&\cdots&1&0&0&0&\cdots&0&0\\
0&0&0&0&0&0&0&0&0&\cdots&0&1&0&0&\cdots&0&0\\
0&0&0&0&0&0&0&0&0&\cdots&0&0&1&0&\cdots&\cdots&\cdots\\
0&0&0&0&0&0&0&0&0&\cdots&0&0&0&1&\cdots&\cdots&\cdots\\
\cdots&\cdots&\cdots&\cdots&\cdots&\cdots&\cdots&\cdots&\cdots&\cdots&\cdots&\cdots&\cdots&\cdots&1&\cdots&\cdots\\
\cdots&\cdots&\cdots&\cdots&\cdots&\cdots&\cdots&\cdots&\cdots&\cdots&\cdots&\cdots&\cdots&\cdots&1&0&0\\
\cdots&\cdots&\cdots&\cdots&\cdots&\cdots&\cdots&\cdots&\cdots&\cdots&\cdots&\cdots&\cdots&\cdots&1&0&0\\
0&0&0&0&0&0&0&0&0&\cdots&0&0&0&0&\cdots&1&0\\
0&0&0&0&0&0&0&0&0&\cdots&0&0&0&0&\cdots&0&1
\end{bmatrix} \tag{31}$$

The periods in the above matrix and in the following matrices signify null elements. The element stiffness matrix and the nodal load vector for the straight element corresponding to the global coordinate system can be obtained via

$$[S_{g2}]^e=[T_{sc}]^T[S_{g1}]^e[T_{sc}] \tag{32}$$

$$\{F_{g2}\}^e=[T_{sc}]^T\{F_{g1}\}^e \tag{33}$$

where $[S_{g1}]$ and $\{F_{g1}\}$ are the stiffness matrix and nodal load vector of the straight element in the local coordinate system.

Next let us consider Fig. 4(c) in which ends a and b of the two intersecting segments do not actually meet. If we connect these points by means of the rigid arm ab, then the transformation matrix $[T_{ra}]$ needed to relate the degrees of freedom at point a in Fig. 5(c) to those at point b is similar to Eqs. (30) and (31) and is listed as follows:

$$[T_{ra}]=\begin{bmatrix}[t_{ra}] & \\ & [t_{ra}]\end{bmatrix} \tag{34}$$

where the submatrix $[t_{ra}]$ is as follows

$$[tra]=\begin{bmatrix}
1&0&0&0&0&\cdots&0&0&\cdots&0&0&0&\cdots&0\\
0&1&0&0&0&\cdots&0&l_a&\cdots&0&0&0&\cdots&0\\
0&0&1&0&0&\cdots&-l_a&0&\cdots&0&0&0&\cdots&0\\
0&0&0&1&0&\cdots&0&0&\cdots&0&0&0&\cdots&0\\
0&0&0&0&1&\cdots&0&0&\cdots&0&0&0&\cdots&0\\
\cdot&\cdot&\cdot&\cdot&\cdot&1&\cdot&\cdot&\cdot&\cdot&\cdot&\cdot&\cdot&\cdot\\
\cdot&\cdot&\cdot&\cdot&\cdot&\cdot&1&\cdot&\cdot&\cdot&\cdot&\cdot&\cdot&\cdot\\
\cdot&\cdot&\cdot&\cdot&\cdot&\cdot&\cdot&1&\cdot&\cdot&\cdot&\cdot&\cdot&\cdot\\
0&0&0&0&0&0&0&0&1&0&\cdots&0&0&0\\
0&0&0&0&0&0&0&0&0&1&\cdots&0&0&0\\
\cdot&\cdot&\cdot&\cdot&\cdot&\cdot&\cdot&\cdot&\cdot&\cdot&1&\cdot&\cdot&\cdot\\
\cdot&\cdot&\cdot&\cdot&\cdot&\cdot&\cdot&\cdot&\cdot&\cdot&\cdot&1&\cdot&\cdot\\
\cdot&\cdot&\cdot&\cdot&\cdot&\cdot&\cdot&\cdot&\cdot&\cdot&\cdot&\cdot&1&\cdot\\
0&0&0&0&0&0&0&0&0&0&0&0&0&1\\
0&0&0&0&0&0&0&0&0&0&0&0&0&1\\
0&0&0&0&0&0&0&0&0&0&0&0&0&1\\
\cdot&\cdot&\cdot&\cdot&\cdot&\cdot&\cdot&\cdot&\cdot&\cdot&\cdot&\cdot&\cdot&\cdot\\
\cdot&\cdot&\cdot&\cdot&\cdot&\cdot&\cdot&\cdot&\cdot&\cdot&\cdot&\cdot&\cdot&\cdot\\
\cdot&\cdot&\cdot&\cdot&\cdot&\cdot&\cdot&\cdot&\cdot&\cdot&\cdot&\cdot&\cdot&\cdot\\
0&0&0&0&0&0&0&0&0&0&0&0&0&1
\end{bmatrix}\qquad(35)$$

in which l_a is the length of the rigid arm connecting a to b. The corresponding element stiffness matrix and nodal load vector are therefore given by

$$[S_g]^e=[T_{ar}]^T[S_{g2}]^e[T_{ar}] \tag{36}$$

$$\{F_g\}^e=[T_{ar}]^T\{F_{g2}\}^e \tag{37}$$

where $[S_{g2}]$ and $\{F_{g2}\}$ are the stiffness matrix and nodal load vector of element 2 in its local coordinate system. For element 1 a similar transformation needs to be applied.

Note that in this particular case the global coordinate system coincides with the local coordinate system of the curved element, thus no coordinate transformation is needed for the stiffness matrix and nodal load vector of the curved element. Once the necessary transformations have been achieved, the process of assembly of the structural stiffness matrix and load vectors proceeds in the usual manner.

The accuracy that can be obtained with the proposed procedure will be demonstrated via the following numerical example.

5. Numerical example

A concrete box girder grillage is analyzed, subjected to one Ontario Highway Bridge Design truck (OHBD Code 1983) on each of the segments 1 and 3, Fig. 5. The box girder has diaphragms only at the supports. It is assumed that the diaphragms endow the box with full torsional and distortional resistance, but with no resistance to warping. The dimensions and loading of the cross section are shown in Fig. 5. As indicated in Fig. 5, a rigid arm is used to model the stiff behaviour of the intersection region. For each of branches 1 and 2, only one straight thin-

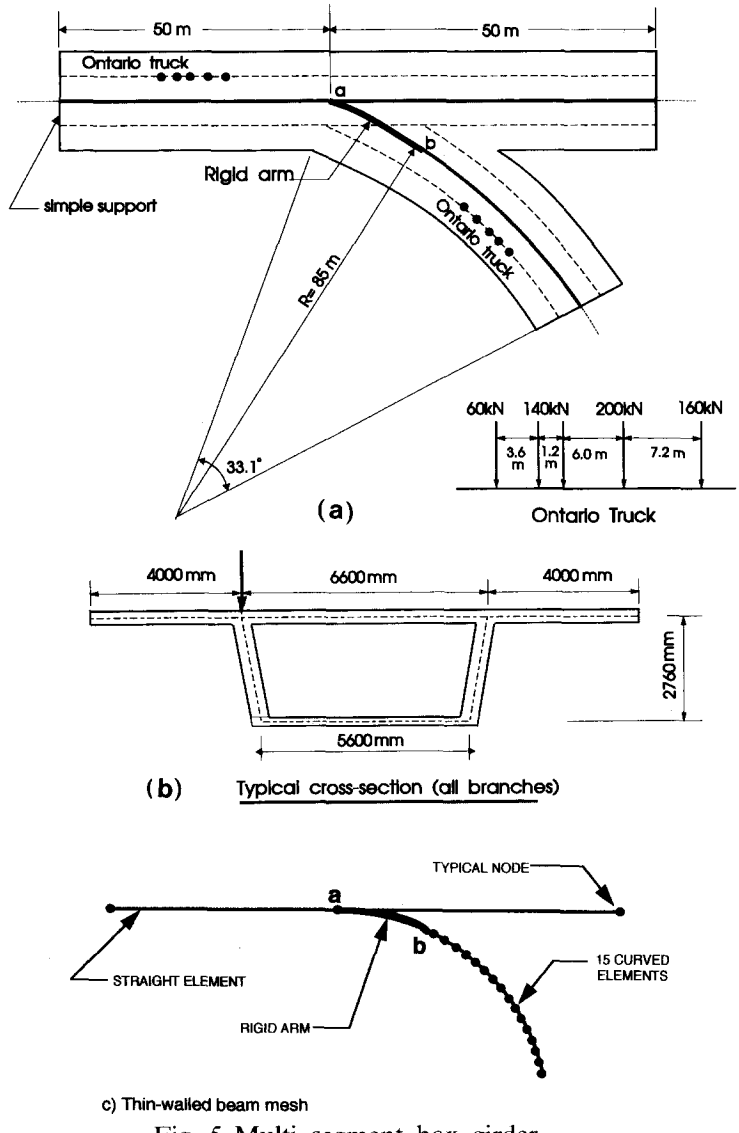

Fig. 5 Multi segment box girder.
(a) Plan, (b) Typical cross section
(c) Finite element mesh

walled box beam element with exact shape functions was used (Razaqpur and Li 1991). For branch 3, fifteen curved thin-walled box beam elements of the type described earlier were used. Facet shell finite analysis was also carried out for the sake of comparison. A total of 268 shell finite elements were used in the analysis, using the program NONLACS (1990).

Figs. 6(a) and 6(b) show the variation along the span of the longitudinal normal stress at junction A, obtained from various beam theories and from the shell finite element analysis. Figs. 7(a) and 7(b) show the longitudinal normal stress due to eccentrically placed trucks at midspan of branches 1 and 3. The results are compared with the shell finite element analysis

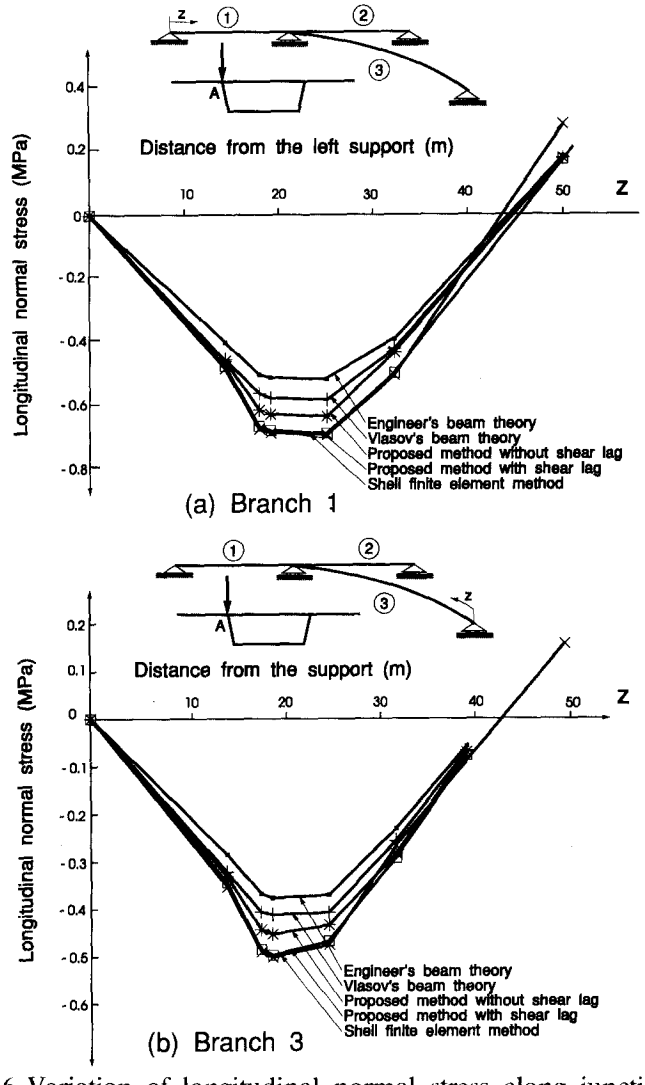

Fig. 6 Variation of longitudinal normal stress along junction A.

and with conventional beam theory. It can be seen that the proposed model results are in good agreement with those of shell finite element, except near the junction of the three members which is not unexpected because the basic theory upon which the present formulation is based can not account for such local effects. On the other hand, the conventional beam theory gives results that differ substantially from the shell finite element results. The maximum error in the normal stresses obtained from conventional beam theory and the proposed thin-walled theory is about 40%.

6. Conclusions

The results in this study show that it is possible to model rather complex three dimensional

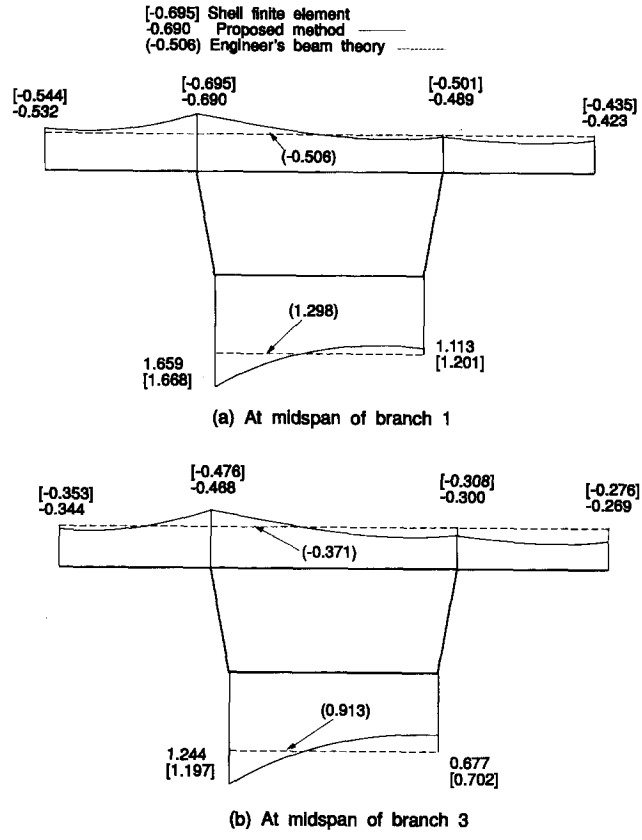

Fig. 7 Longitudinal normal stress at different cross-sections of box girder assemblage.

box girder assemblages as a grillage of box beam elements. The proposed method applies to both straight and curvedbox girders. The key to the accuracy of the results is consideration of all the significant deformation modes of thin-walled box girders, including torsional warping, distortion, distortional warping, and shearlag. Also, realistic idealization of the intersection regions of non-colinear box girder segments, and the proper imposition of the compatibility requirements in those regions would lead to improved assessment of the state of stresses and deformations in the box girder segments. The preceding conclusions are based on the comparison of results from the proposed method with those obtained from thin shell finite element analyses. Neglecting the foregoing effects, as in conventional beam theory,can introduce significant error in the magnitude and distribution of longitudinal normal stresses.

Acknowledgements

The authors are grateful for the financial assistance of the Natural Sciences and Engineering Research-Council of Canada (NSERC) in support of the research presented in this paper.

References

Bazant, Z. P. and El Nimeiri, M. (1974), "Stiffness method for curved box girders at initial stress", *J. of Struct. Engrg., ASCE,* **100**(10), 2071-2090.

Li, G. H. (1987), "Analysis of box girder and truss bridges", Springer Veralg, Berlin

Mikkola, M. J. and Paavola, J. (1980). "Finite element analysis of box girder", *J. of Struct. Engrg., ASCE,* **106**(6), 1343-1356.

OHBD code, (1983). *Ontario highway bridge design code.* Ministry of Transportation of Ontario, Downsview, Ontario, Canada.

Razaqpur, A. G. and Li, H. G. (1994). "Curved thin-walled multicell box girder finite element", *J. of Computer and Struct.,* **53**(1), 131-142.

Razaqpur, A. G. and Li, H. G. (1991). "Thin-walled multicell box girder finite element", *J. of Struct. Engrg., ASCE,* **117**(10), 2953-22971.

Razaqpur, A. G. and Li, H. G. (1990). "Analysis of multi-branch multi-cell box girder bridges", *Proceedings of the Third International Conference* on Short andMedium Span Bridges, Toronto, Canada, 153-164.

Razaqpur, A. G. and Nofal, M. (1990), "Analytical modelling of nonlinear behaviour of composite bridges", *J. of Struct. Eng.,* **116**(6), 1715-1733.

Reissner, E. (1938), "On the problem of stress distribution in wide-flanged box-beams", *J. of Aero Sci.,* **5**(8), 295-299.

Roik, K. and Sedlacek, G. (1970), "Extension of engineer's theory of bending and torsion, considering shear deformation", *Die Bautechnik.* **47**(1), 20-30 (in German).

Sedlacek, G. (1968), *Systematic Description of the Process of Bending and Torsion for Prismatic Beams of Thin-Walled Cross-Section, Considering Distortion of Cross-Section,* Fortschritt-Berichte VDI-Zeitschrift, Reihe 4, Nr. 8, September 1968, 110 (in German).

Zhang, S. H. and Lyon, L. P. R. (1984), "A thin-walled box beam finite element for curved bridge analysis", *J. of Computer and Struct.,* **18**(6), 1035-1046.